SOLAR-B Instrument

EIS MTM/TTM THERMAL BALANCE TEST STEADY-STATE RESULTS AND CONCLUSIONS

Document No. BU/SLB-EIS/TN/028.01

Compiled by H. Mapson-Menard

The University of Birmingham
Astrophysics and Space Research Group
01/05/02

EIS MTM/TTM THERMAL BALANCE TEST STEADY-STATE RESULTS AND CONCLUSIONS

INTRODUCTION

This document describes the results and conclusions of the thermal balance tests performed on the EUV Imaging Spectrometer Mechanical/Thermal Test Model. The tests were carried out in the Rutherford Appleton Laboratory Space Test Chamber on 27/02/02 - 03/03/02 inclusive. Hot operational steady-state, cold non-operational steady-state and hot to cold transient tests were performed and temperatures recorded with a frequency of once per minute. Thirteen heater mats and seven heater resistors were used to control the temperature of the structure and components (respectively), and to simulate the external power loads predicted in orbit.

See documents BU/SLB-EIS/TN/020.03, EIS MTM/TTM Thermal Balance Test Specification, Procedures and Predictions, and BU/SLB-EIS/PS/004.01, EIS MTM/TTM Thermal Test Preparations and Procedures, for more information.

TEST OBJECTIVES

- To determine the effective conductivity of the MLI
- To verify the thermal mathematical model

The objective was not to reproduce exact orbital temperature distributions, but to achieve equilibrium in two steady-state cases. Therefore, heaters were set at pre-determined dissipation values and the structure was allowed to come to the resulting equilibrium temperatures. Any discrepancies between the actual and predicted temperatures resulted in adjustments to the thermal mathematical model.

TEST RESULTS

The results are presented in a schematic format for clarity. Figure 1 explains the schematic, which shows the important optical bench and component nodes. Figures 2 and 3 show the hot and cold test equilibrium temperatures. Figures 4 and 5 show the thermal mathematical model predictions for the hot and cold tests.

Table 1 describes the sensor positions. The test and thermal model results for all sensors are shown in Graphs 1 and 2 for the hot and cold test cases respectively.

Figure 1: Explanation of the Thermal Results Schematic

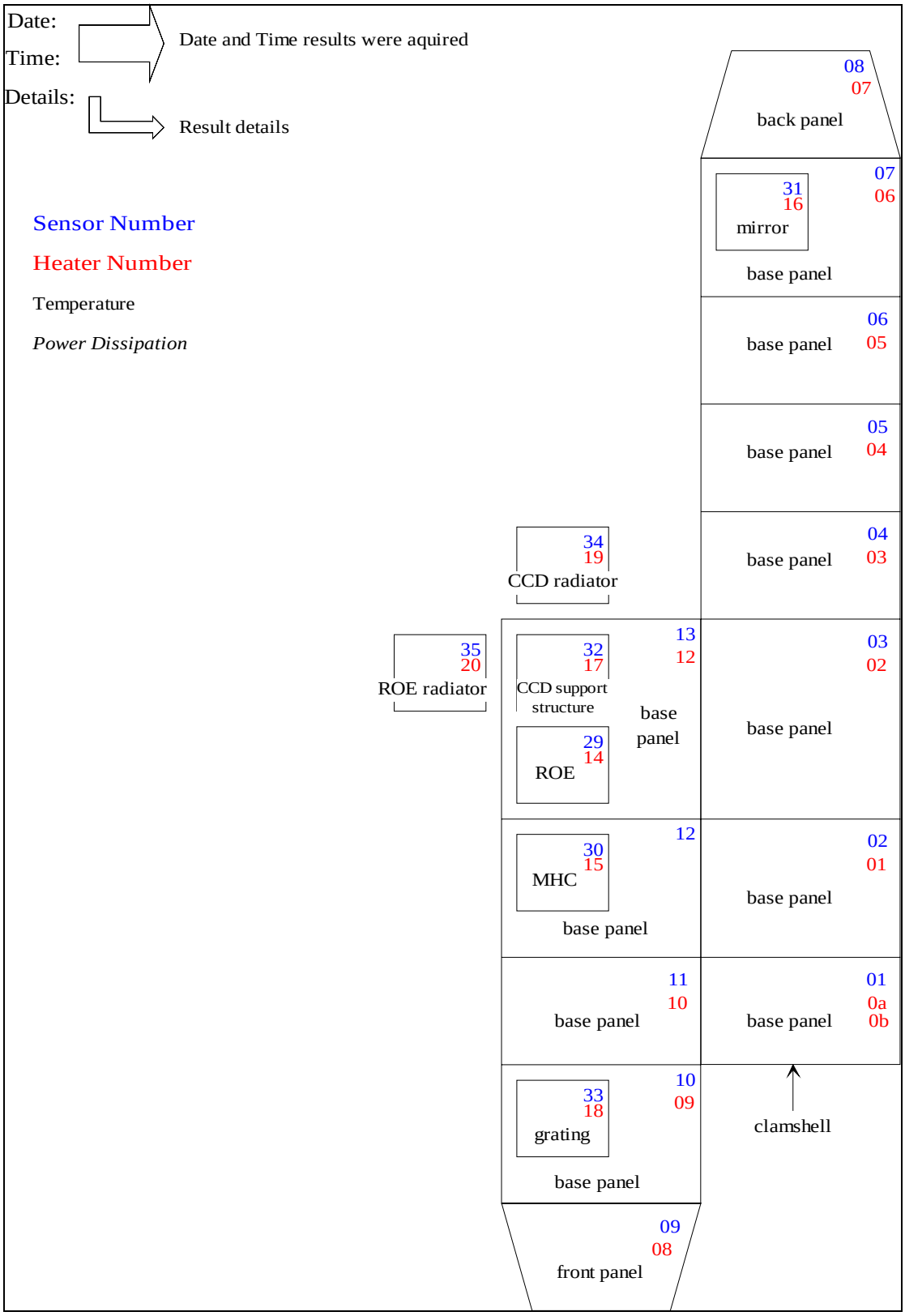

Figure 2: Hot Test Equilibrium Temperatures

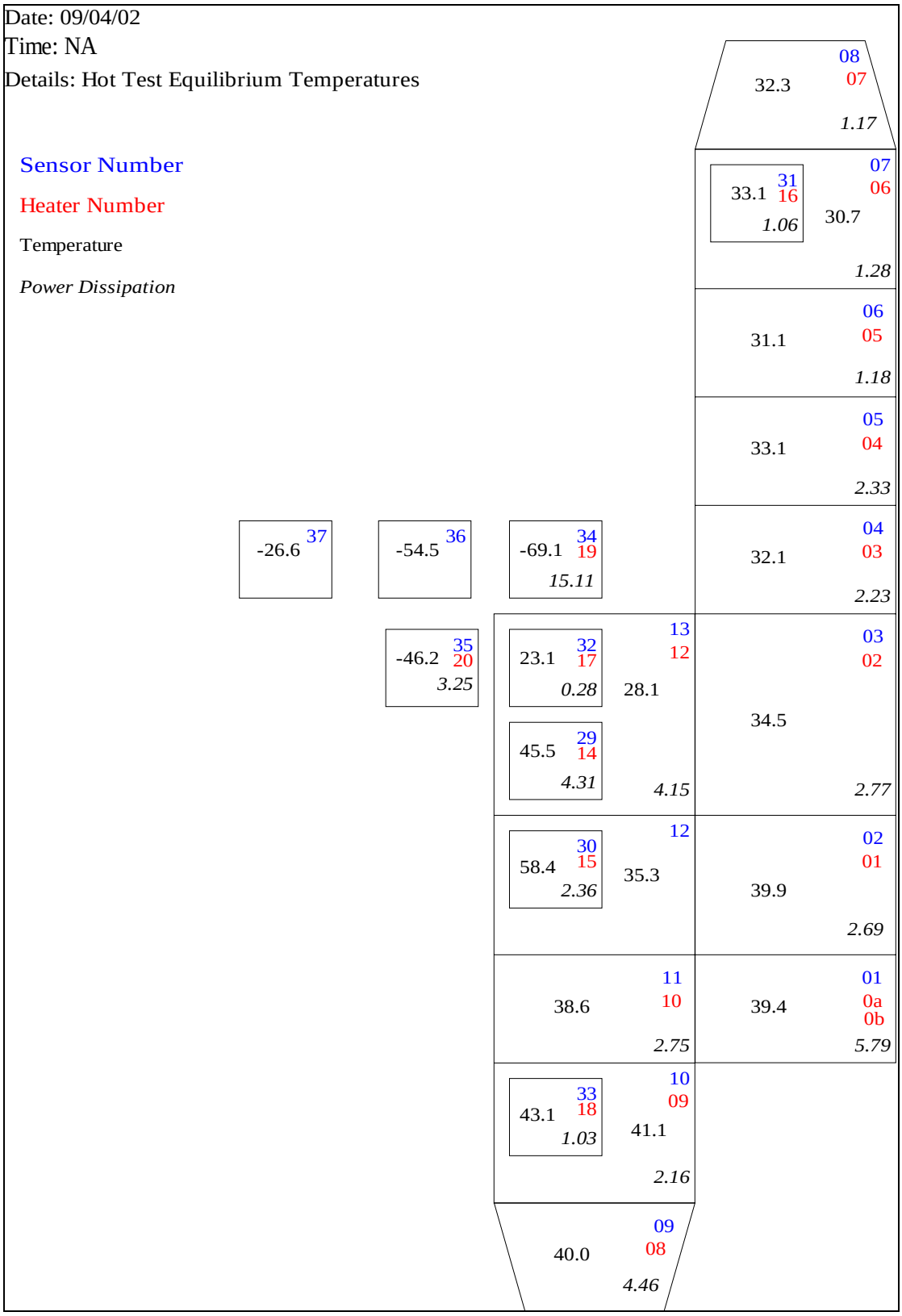

Figure 3: Cold Test Equilibrium Temperatures

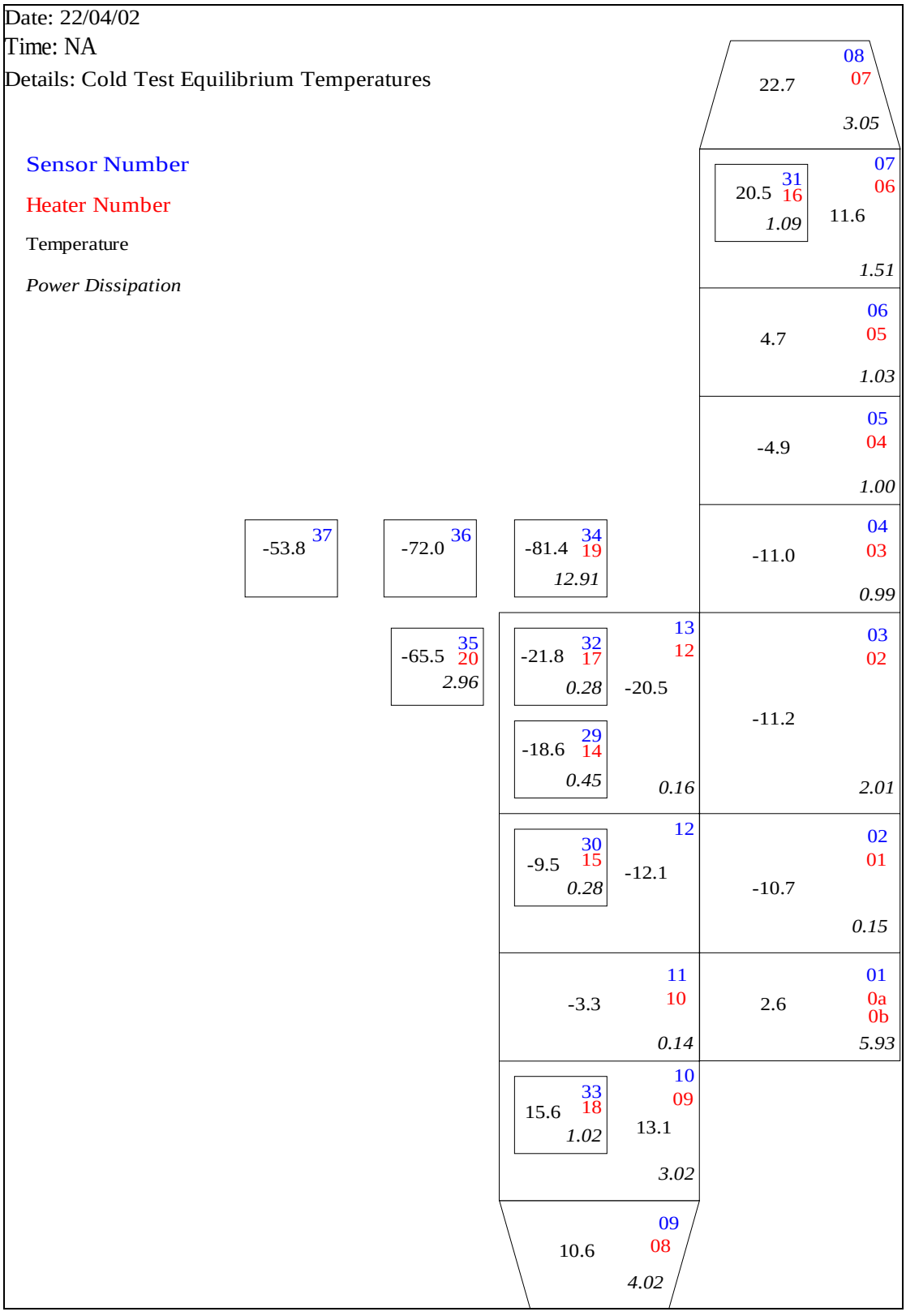

Figure 4: Hot Test Thermal Model Predicted Temperatures

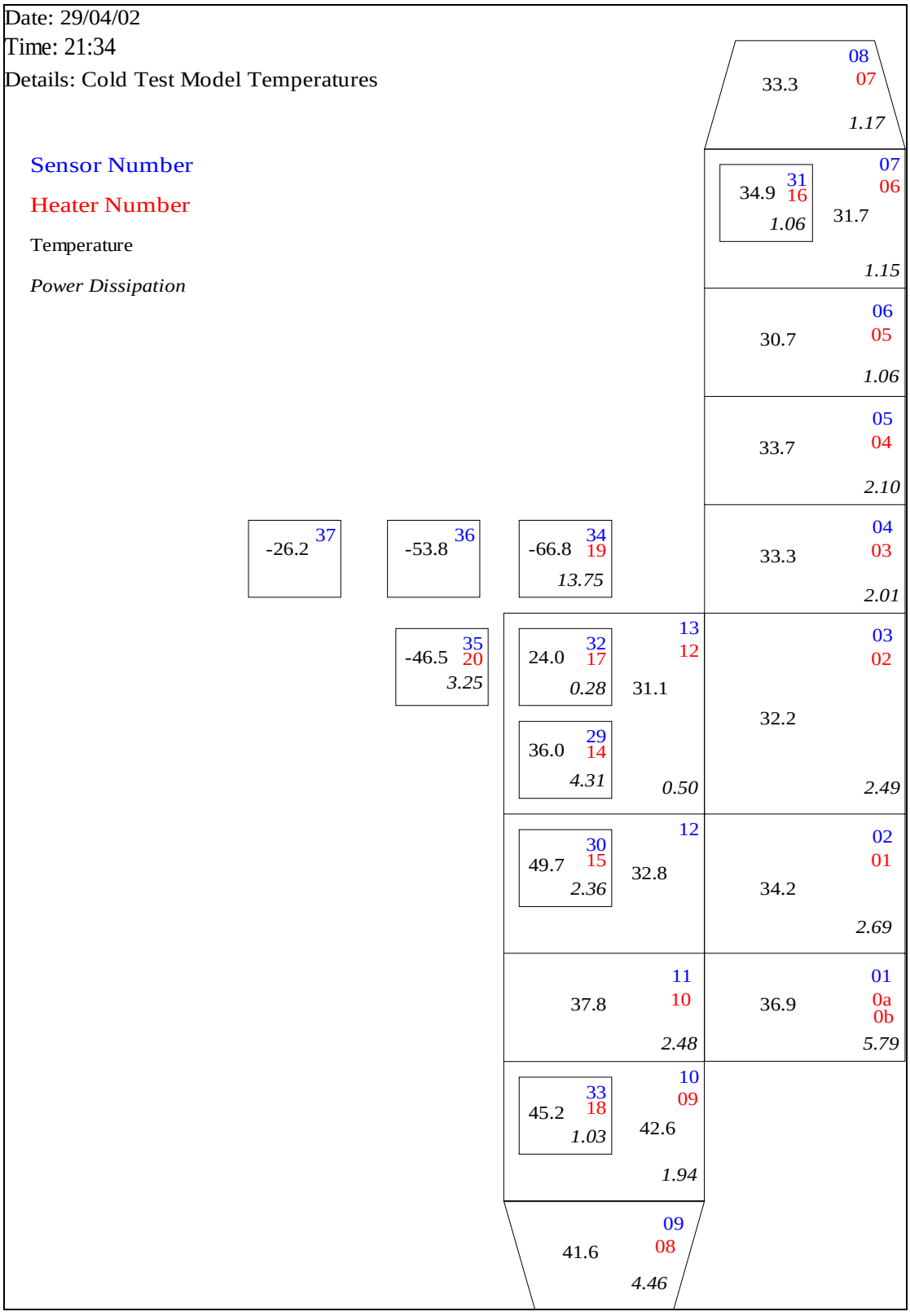

Figure 5: Cold Test Thermal Model Predicted Temperatures

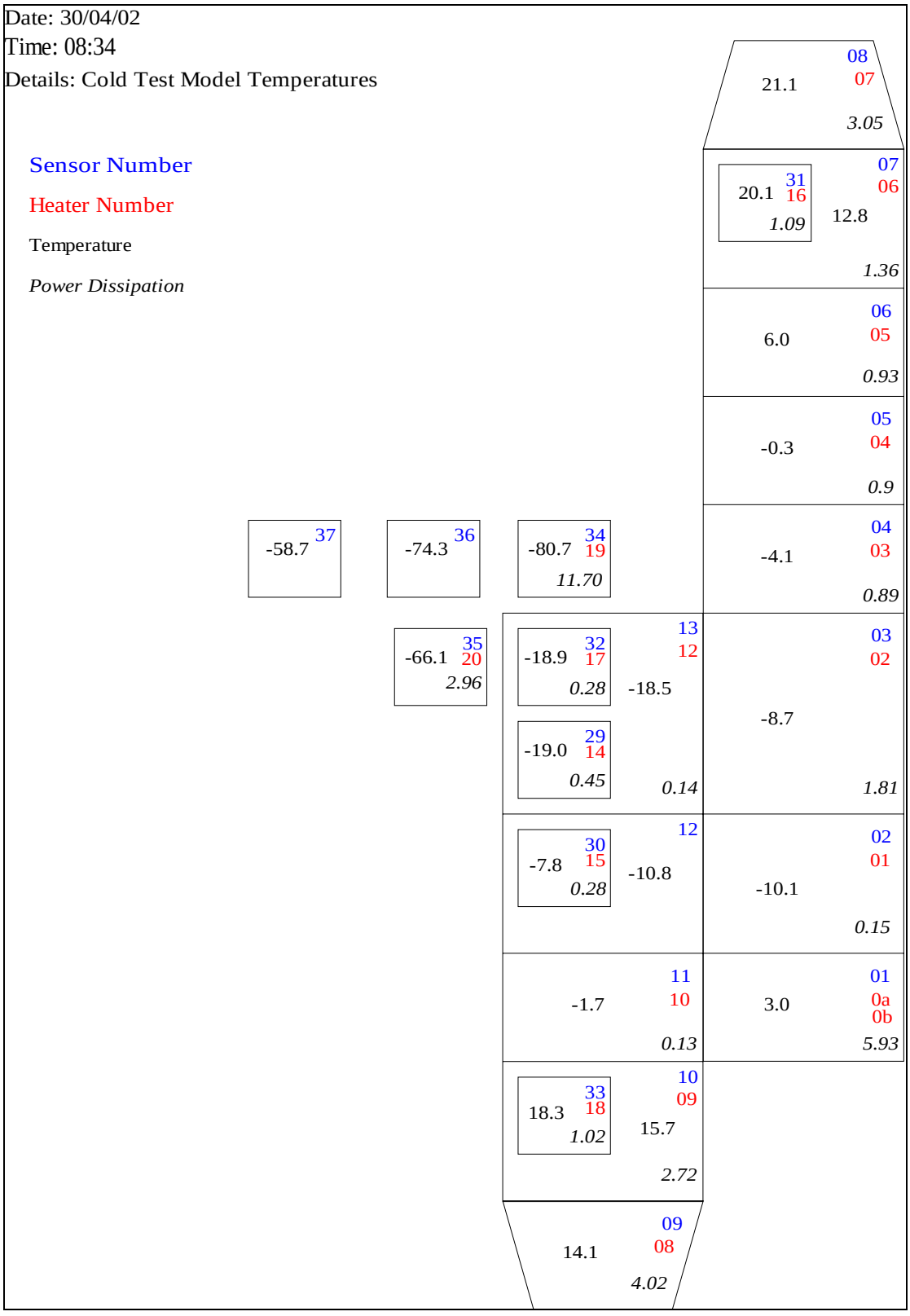

Table 1: Thermal Sensor Descriptions

Sensor Name	Thermal Node	Description of Position
EIS-TTS-01	6032	Inside, P1 +Y face bt P2, P12A0, P13, P9
EIS-TTS-02	6011	Inside, P1 +Y face bt P2, P13, P14, P10
EIS-TTS-03	6009	Inside, P1 +Y face bt P2, P14, P15, P11
EIS-TTS-04	6050	Inside, P1 +Y face bt P2, P15, P16, P3
EIS-TTS-05	6049	Inside, P1 +Y face bt P2, P15, P16, P3
EIS-TTS-06	6048	Inside, P1 +Y face bt P2, P16, P7, P3
EIS-TTS-07	6047	Inside, P1 +Y face bt P2, P16, P7, P3
EIS-TTS-08	6059	Inside, P7 +Z face centre
EIS-TTS-09	6028	Inside, P8 -Z face centre
EIS-TTS-10	6025	Inside, P1 +Y face bt P9, P8, P12C0, P4
EIS-TTS-11	6024	Inside, P1 +Y face bt P9, P12CO, P13, P4
EIS-TTS-12	6012	Inside, P1 +Y face bt P10, P13, P14, P4
EIS-TTS-13	6010	Inside, P1 +Y face bt P11, P14, P15, P4
EIS-TTS-14	6044	Outside, P5 +Y face bt P2, P16, P7, P3
EIS-TTS-15	6014	Outside, P6 +Y face bt P2, P13, P14, P10
EIS-TTS-16	6034	Outside, P6 +Y face bt P2, P12A0, P13, P9
EIS-TTS-17	6027	Outside, P6 +Y face bt P9, P8, P12CO, P4
EIS-TTS-18	6144	On P5 MLI, bt P2, P16, P7, P3
EIS-TTS-19	6114	On P6 MLI, bt P2, P13, P14, P10
EIS-TTS-20	6134	On P6 MLI, bt P2, P12A0, P13, P9
EIS-TTS-21	6127	On P6 MLI, bt P9, P8, P12C0, P4
EIS-TTS-22	6159	On P7 MLI, centre
EIS-TTS-23	6128	On P8 MLI, centre
EIS-TTS-24	6152	On P2 MLI, bt PP16, P7, P1, P5
EIS-TTS-25	6106	On P2 MLI, bt P13, P14, P1, P6
EIS-TTS-26	6130	On P2 MLI, bt P12A0, P13, P1, P6
EIS-TTS-27	6121	On P4 MLI, bt P8, P12CO, P1, P6
EIS-TTS-28	6112	On P1 MLI, bt P10, P13, P14, P4
EIS-TTS-29	6079	ROE structure
EIS-TTS-30	6065	MHC structure
EIS-TTS-31	6063	Mirror centre
EIS-TTS-32	6070	CCD
EIS-TTS-33	6064	Grating centre
EIS-TTS-34	6065	CCD radiator
EIS-TTS-35	6076	ROE radiator
EIS-TTS-36	6073	Particle shield top
EIS-TTS-37	6080	Particle shield bottom

Graph 1: Complete Hot Test Temperature Results and Predictions

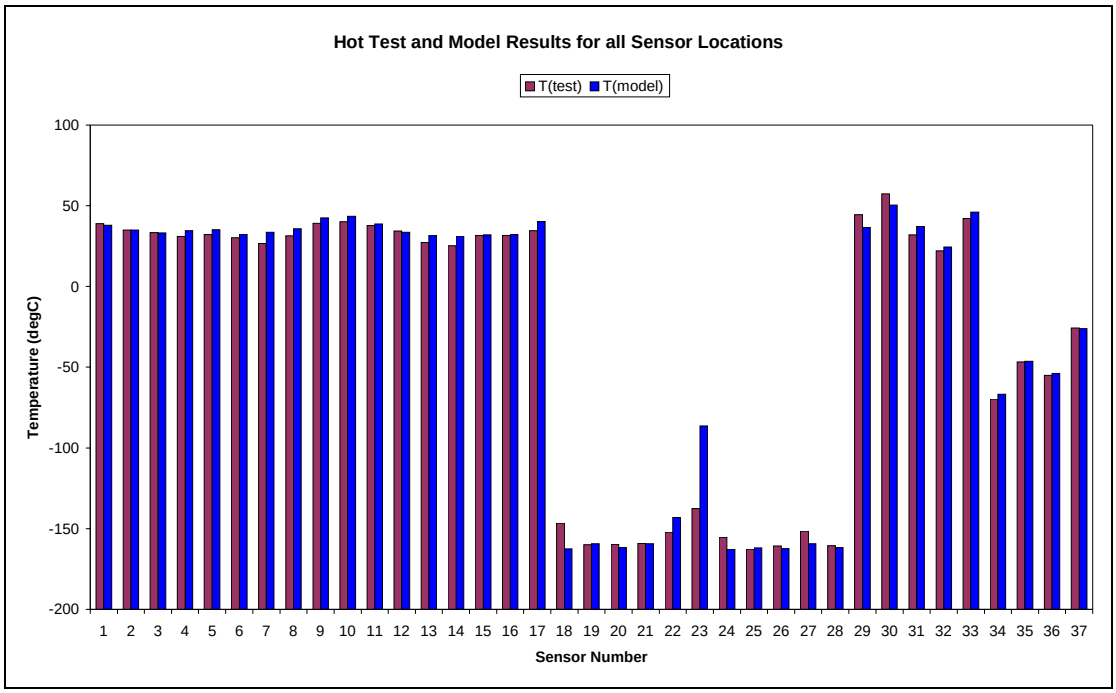

Graph 2: Complete Cold Test Temperature Results and Predictions

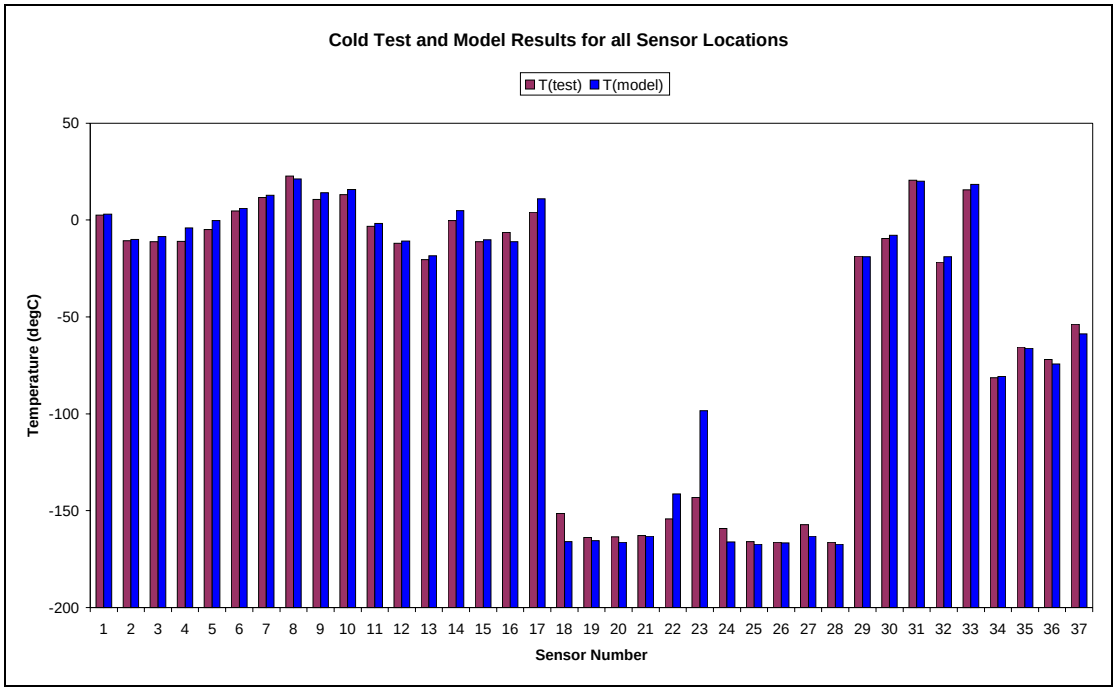

DISCREPANCIES BETWEEN TEST AND MODEL RESULTS

INTRODUCTION

The thermal model was adjusted so it predicted similar temperatures and trends as the thermal test results showed. However, some temperatures could not be made to correlate effectively. This section discusses the reasons behind significant discrepancies of more than 5°C.

FRONT MLI TEMPERATURE

The thermal model predicts a temperature ~50°C warmer than the results from sensor 23, the front MLI section, in both the hot and cold tests. The efficiency of this MLI section has been greatly reduced to 0.29 $Wm^{-2}K^{-1}$, to allow the corresponding structural areas to reach realistic temperatures. This means that a larger amount of power is being radiated from this area than is indicated by the MLI temperature. Figure 6 shows the front of EIS during pre-test preparations. The position of the sensor in question can be seen (under the small section of black kapton tape). Also shown are gaps in the MLI where flaps have been created to allow the protrusion of the lifting eyebolt interface. It is believed that power is being dissipated from the structure through these gap areas and not via the MLI. The thermal model geometry includes this whole front section as one node (not including the aperture half), so any power being radiated from the area will be seen to travel via the MLI as the gaps are not featured in the geometry. The more power the MLI radiates, the warmer it will be, so the higher model temperature represent the power being radiated through the gaps.

Figure 6: The Front MLI Section of EIS

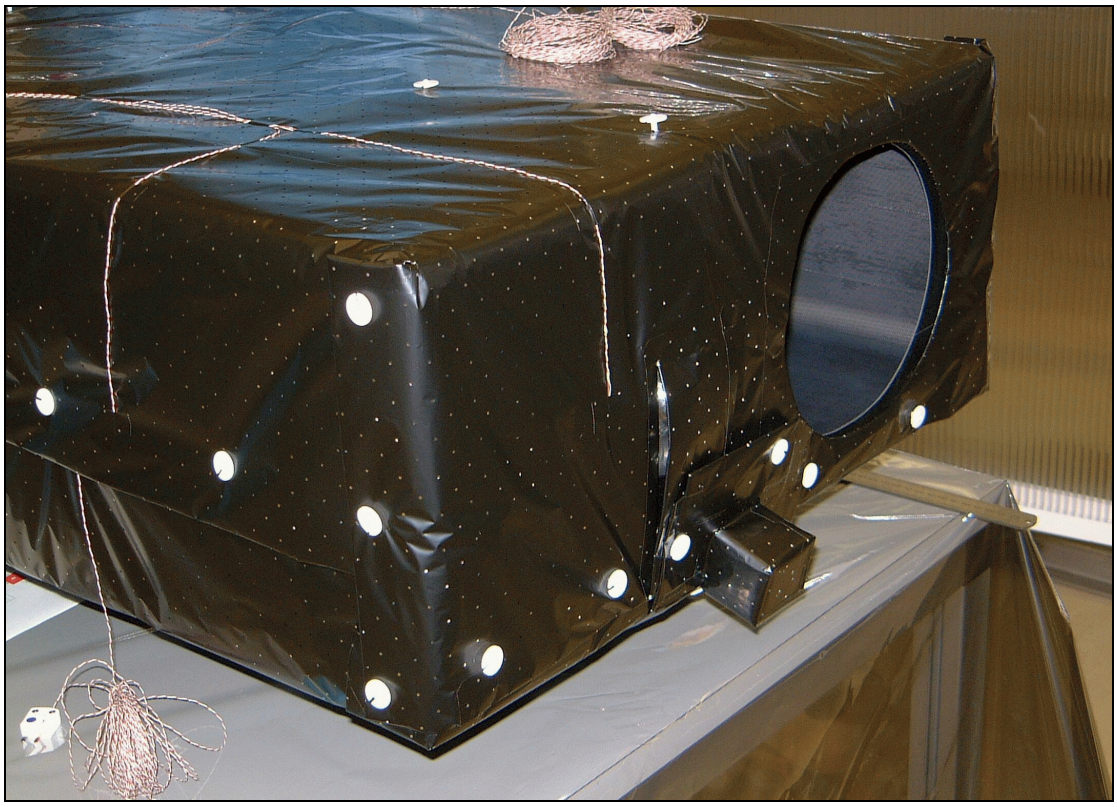

BACK MLI TEMPERATURE

The thermal model predicts a temperature ~10°C warmer than the results from sensor 22, the back MLI section, in both the hot and cold tests. Figure 7 shows gaping regions of the MLI where overlaps are made in this section. It is believed that the sensor shows the MLI itself is working efficiently, but that power is being radiated from the gaping areas.

Figure 7: The Back MLI Section of EIS

TOP CENTRAL MIRROR TUBE MLI TEMPERATURE

The thermal model predicts a lower temperature for the top central mirror tube MLI section, for the hot and cold tests (sensor 18). It is believed that this is due to sensor 18 being placed close to the MLI hole for the purge vent. The purge vent is an aluminium component placed in the top panel. The proximity of the MLI temperature sensor to the MLI hole means that it is less effective in this localised region, and hence radiating more power than normal. The corresponding structure results (sensor 14) show that the overall performance of the MLI is still good.

MODIFICATIONS MADE TO THE MATHEMATICAL MODEL SO THE THERMAL TEST RESULTS ARE REPRESENTED

Document BU/SLB-EIS/TN/020.03, EIS MTM/TTM Thermal Balance Test Specification (Appendix 1), lists the changes that were initially made to convert the model from FM to MTM/TTM. Below, Table 2 lists the conductive links that were individually modified.

- Structure emissivity reduced from 0.9 to 0.75. Allowed the front optical bench area (sensor 01) to reach the required temperatures.
- General MLI effective conductivity reduced by a factor of 0.6. Increased the overall temperature. Represents excellent MLI performance.
- Front section MLI effective conductivity increased by a factor of 7.5. Represents MLI degradation due to overlaps and eyebolt interface flaps.
- Back section of MLI effective conductivity increased by a factor of 2.0. Represents MLI degradation due to overlaps.
- Central MLI section effective conductivity reduced by a factor of 0.55. Represents even better MLI performance in areas without holes or folds.
- Structure conductivity reduced by a factor of 2.5. Increased temperature gradients.
- Front bulkhead split into two nodes representing a gradient between the front and rear panel skins.
- Baffle split into 9 additional nodes so that gradients in the X-axis, as well as the Z-axis, could be represented.
- Most heater mat power dissipations were reduced by 10%. The exceptions were heaters 0a, 0b, 1, 7 and 8 as these were integrated with a more successful method that will be used for flight heaters.
- Heater 12 power dissipation reduced by 3W in the hot test. Power loss could be due to summation of numerous effects, such as:
  - power drawn to CCD cold cone, as the protective foils are not present
  - power drawn to ROE cooling system, as the system does not feature the preferred surface finishes or protective foils
  - ineffective power transmission to the structure itself, due to “bumpy”, resin-rich local thickening reducing surface contact with the heater
  - power loss to harness
- CCD radiator heater resistor dissipation reduced by 9%. Represented power dissipated to STC (and not conducted to radiator).

Table 2: Modified Conductive Links

Node I	Node J	New Value (W/K)	Original Value (W/K)	Description
6036	6019	0.4	N/A	Linking front (clamshell) bulkhead front and rear skins
6059	6047	0.05	N/A	Linking rear panel to rear mirror tube base
6028	6025	0.3	N/A	Linking front panel to base panel
6028	6023	0.3	N/A	Linking front panel to side panel
6028	6021	0.3	N/A	Linking front panel to side panel
6063	6059	0.15	0.1	Mirror to structure link
6064	6025	0.25	0.1	Grating to structure link
6065	6012	0.01	1	MHC to structure link

THERMAL SENSITIVITIES AND IMPLICATIONS

MHC LINK TO STRUCTURE

10% link reduction => ~6°C MHC temperature increase
=> ~1°C mounting structure temperature decrease

The MTM/TTM conductive link was significantly reduced, creating a large gradient between the MHC and its mounting structure. This interface should be better coupled.

MHC OUTER SURFACE FINISH

The sensitivity of the MHC temperature to its outer box optical properties varies with temperature. The MHC box should therefore have a black finish so the maximum power coupling with the structure is achieved.

ROE LINK TO STRUCTURE

0.01W/K link decrease => 1°C ROE box temperature increase

Due to dominant radiative control within the EIS structural enclosure, the optical properties of the ROE box have little affect on the ROE temperature when T(ROE) ~ T(structure). However, as the above figures show, when the ROE is 10°C warmer than the structure, the link plays a significant role in determining the ROE operating temperature.

ROE OUTER SURFACE FINISH

Correct surface finishes => T(ROE) = 29°C
Plain aluminium finish => T(ROE) = 45°C

To minimise the power load on the ROE cooling system, the correct surface finishes should be produced. The optical properties assumed in the thermal model (to produce the 29°C hot case operating temperature) are:

$\alpha = 0.1$ $\varepsilon = 0.05$ for general surfaces, and
$\alpha = 0.9$ $\varepsilon = 0.9$ for the top surface that views the base of the thermal shield

The thermal shield connected to the ROE radiator should have similar optical properties.

INTERNAL HEATER POWER (TEST CONFIGURATION)

1W power increase => 2°C general temperature increase
=> 4°C temperature increase in area of power increase

OPTICAL PROPERTIES OF THE STRUCTURE

Graph 3 shows the normalised variation of two node temperatures with structure emissivity. The nodes featured correspond to the base plate area immediately behind the clamshell (6032) and the front panel in front of the grating (6028). Reducing the emissivity also had the affect of increasing the gradients across the structure. It is unlikely that the structure has $\varepsilon < 0.75$. Higher values of ε did not produce the high temperatures witnessed behind the clamshell during the tests.

Graph 3: Node Temperature Variation with Structure Emissivity

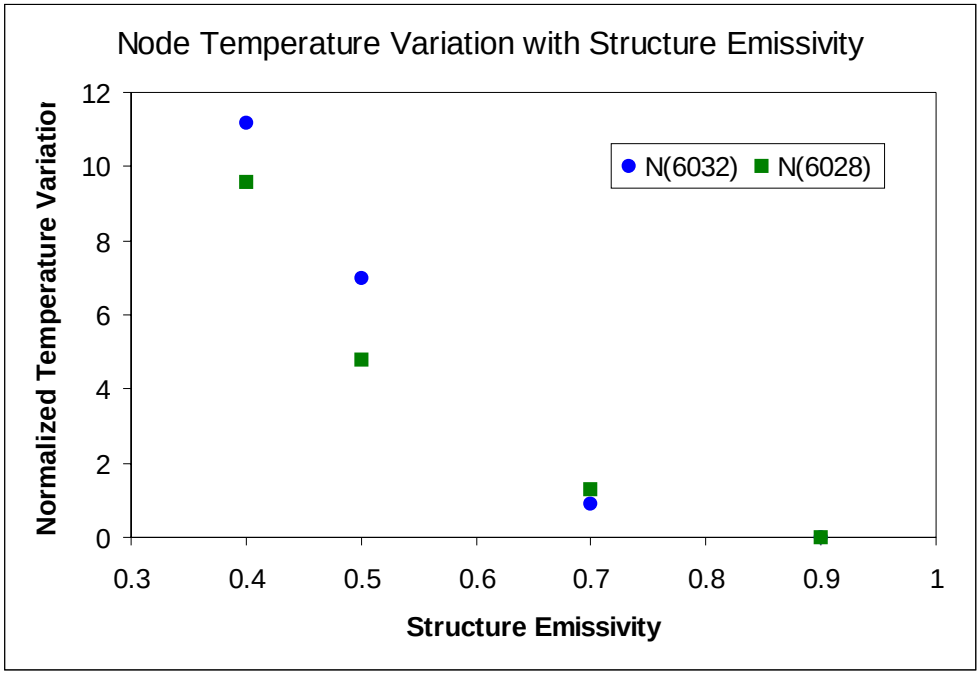

MLI PERFORMANCE

The MLI performance was better than predicted. ESA MLI efficiency tables predicted ~0.039 $Wm^{-2}K^{-1}$ for good quality, large blankets with an average structure and MLI temperature of ~210K. The MLI conductivity predicted by the thermal model, to generate the correct test temperature results, was ≤ 0.02 $Wm^{-2}K^{-1}$, except areas with overlaps and holes. This value was verified by calculating the power radiated from sections of the MLI using the MLI temperatures recorded during the hot and cold tests. This was then used to calculate the link required for the power to be conducted through the specified area of MLI. The conductive link required was also found to be ≤ 0.02 $Wm^{-2}K^{-1}$.

THERMAL MATHEMATICAL MODEL TEMPERATURE PREDICTIONS FOR THE EIS FLIGHT MODEL

The adjusted EIS thermal model was modelled in orbit for the hot operating, cold operating and 25° hot survival environment cases. This highlighted any problems caused by the adjustments made to the model. Figures 8, 9 and 10 show the predicted in flight temperatures for the cases listed above. The models were modified so that the expected surface finishes were on all components. Also, the effective conductivity of the front MLI node was reduced to 0.078 $Wm^{-2}K^{-1}$ (from 0.29 $Wm^{-2}K^{-1}$). No other conductive links were adjusted from the MTM results model.

Figure 8: Hot Operational Case Thermal Model Predicted Temperatures

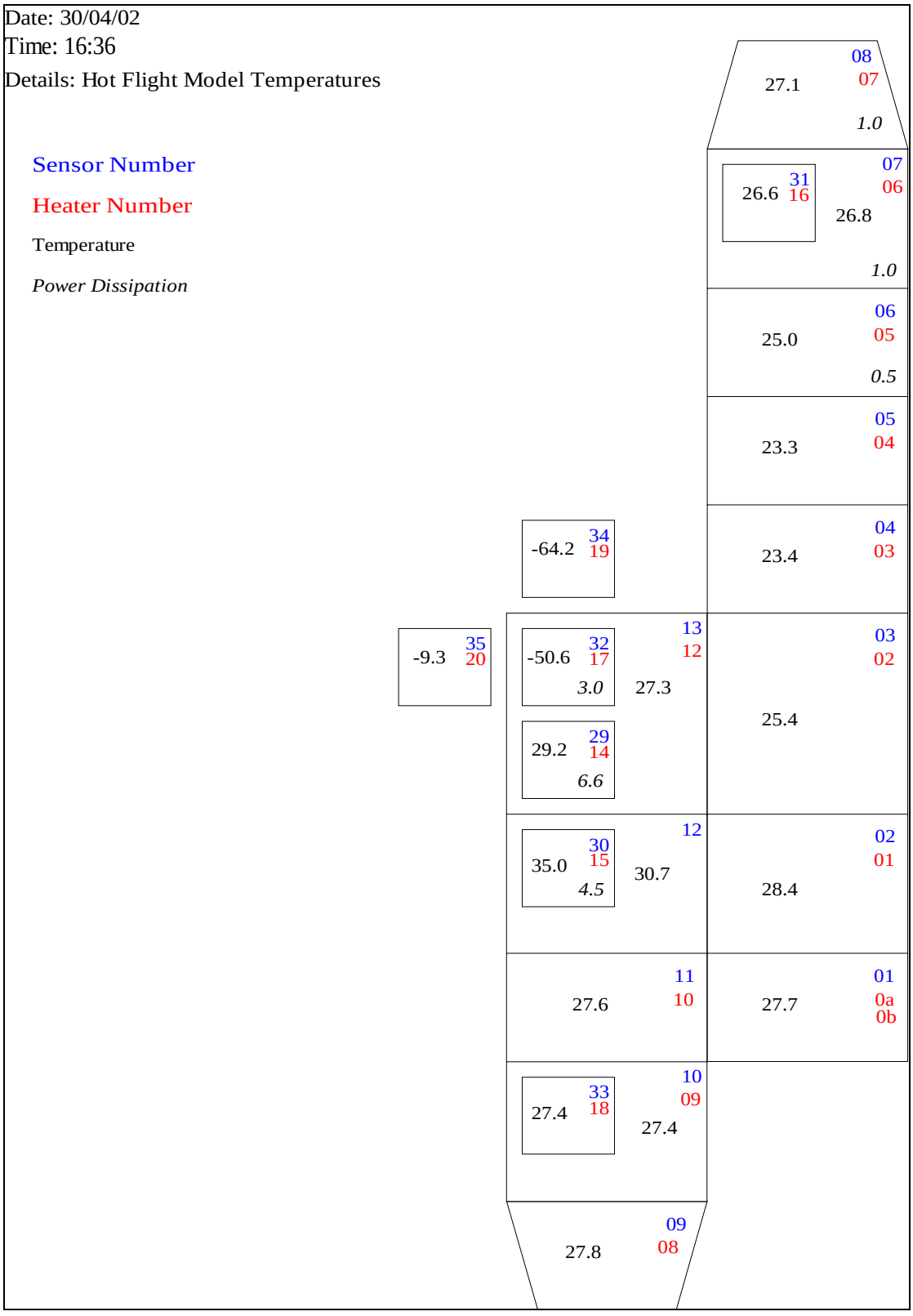

Figure 9: Cold Operational Case Thermal Model Predicted Temperatures

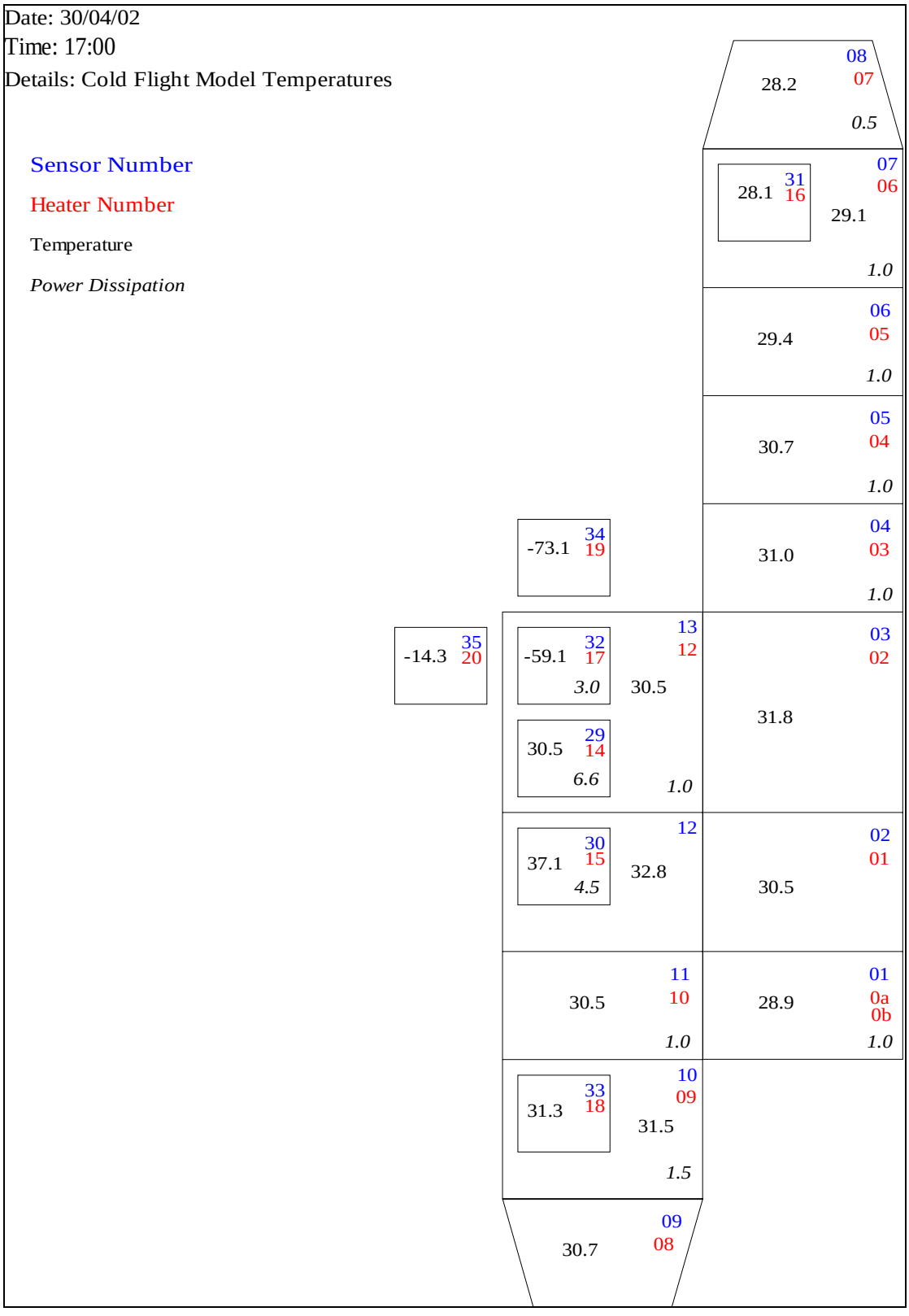

Figure 10: Hot 25° Survival Case Thermal Model Predicted Temperatures

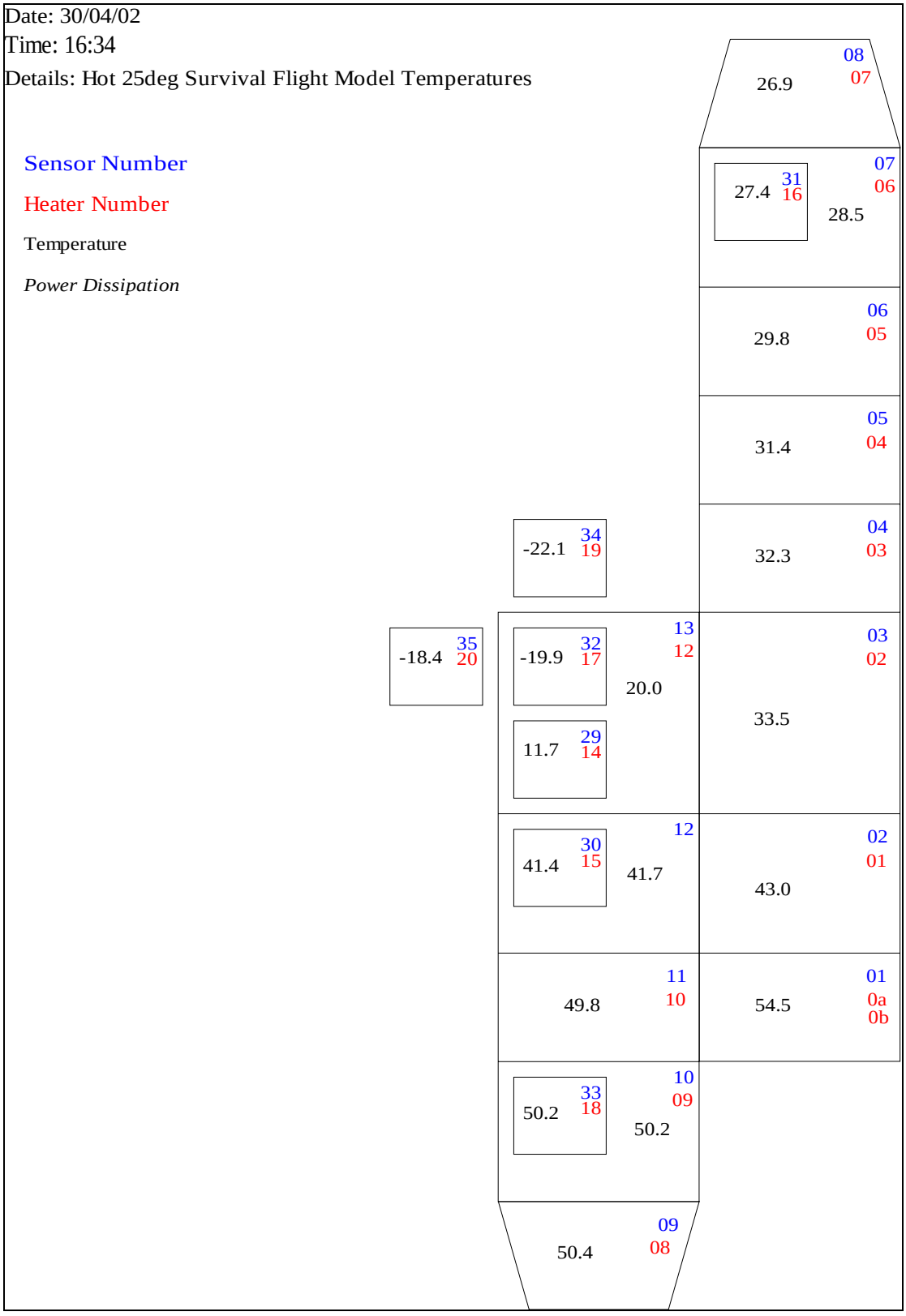

CONCLUSIONS

The EIS MTM/TTM thermal balance tests were successful. The effective conductivity of the MLI was found to be ≤ 0.02 $Wm^{-2}K^{-1}$. The thermal model was adjusted so it predicted the equilibrium temperatures, in both the hot and cold test cases, within ± 5°C. The main differences between the original and adjusted thermal models were the improved MLI performance, the structure optical properties, the conductivity of the panels, and the conductive links between components. Discrepancies, larger than 5°C, between the test results and thermal model predictions were found to be caused by temperature sensor placements and model resolution - not the assumptions used within the model. It was therefore found that the thermal mathematical model was verified.

The CCD temperature sensor had not been placed on/near a CCD, but on the CCD support structure, so the CCD cooling path was not verified past the CCD radiator and particle shield. A sensor has now been placed on a CCD, so the conductivity of the braid connecting the upper particle shield and CCD can be verified during system thermal tests.

It was concluded that some modifications should be made to the EIS Flight Model to optimise performance. These are listed below.

MODIFICATIONS REQUIRED FOR THE FLIGHT MODEL

- Larger MLI overlaps, to ensure consistent MLI performance in joint regions.
- An extra section of MLI to cover the eyebolt interface, to improve the front section MLI performance.
- Possible MLI layer reduction, to reduce the hot case operational temperatures.
- Better contact (larger thermal link) between the MHC and the structure, to keep the MHC operating temperature to a minimum.
- Dark MHC surface finish, to keep the MHC operating temperature to a minimum.
- Correct ROE box and cooling system optical finishes, to insure minimal heat loads on the ROE cooling system from the structure.